2-D EM Scattering and Inverse Scattering From Inhomogeneous Objects Straddling Multiple Subsurface Planar Layers With a Rough Surface

Qing Wu, Ruidong Huang, and Feng Han, *Senior Member, IEEE*

Abstract— This letter presents the computation of electromagnetic (EM) forward scattering from and the full-wave inversion (FWI) of 2-D inhomogeneous scatterers straddling multiple subsurface planar layers covered by 1-D locally rough surface. In the forward scattering, the electric field integral equation (EFIE) is formulated and the 2-D Green's functions are evaluated by the transmission-line analogy method and the buried object approach (BOA) to account for both the reflection and transmission in the multiple planar layer boundaries and the random scattering from the locally rough surface. The computation accuracy of the forward solver is verified by comparing the simulation results with the finite element method (FEM) outcomes. Meanwhile, the additional computational cost caused by the rough surface is investigated in numerical experiments and also explained in theory. It is shown that, for the numerical case in this letter, the forward solver needs nearly 90 times computation time and consumes nearly 30 times memory when the rough surface is present compared with those when it is absent. Meanwhile, In FWI, the variational Born iterative method (VBIM) is adopted to reconstruct multiple scatterers straddling multiple subsurface planar layers when the rough surface is present or absent. Numerical experiments show that neglecting a rough surface with the root mean square (rms) height of 0.1 m almost causes the failure of the inversion.

Index Terms— Buried object approach (BOA), electromagnetic (EM) scattering, inverse scattering, multilayered media, rough surface.

I. INTRODUCTION

THE research of electromagnetic (EM) scattering and inverse scattering has a long history. It started from the analytical computation of plane wave scattering by a simple sphere [1] and was later extended to numerical solutions of more complicated configurations, e.g., irregular scatterers with anisotropic parameters [2]. Typical applications include microwave imaging [3] and geophysical exploration [4], etc.

One of the most commonly used methods to solve EM scattering and inverse scattering problems is using integral equations (IEs). However, the original method of moment (MoM) to solve the discretized IEs has an unaffordable computational cost [5]. A large class of improved fast algorithms is using the fast Fourier transform (FFT) to accelerate the integration of the multiplication of the equivalent current and Green's functions. Representative methods include biconjugate gradient FFT (BCG-FFT) [6], stabilized BCG-FFT (BCGS-FFT) [7], etc. These forward scattering approaches have been combined with full-wave inversion (FWI) methods such as the variational Born iterative method (VBIM) to reconstruct 2-D or 3-D scatterers placed inside a homogeneous medium [8] or buried in planarly multilayered media [9]. The successful applications of these forward or inverse scattering computational methods highly depend on the availability of Green's functions, either by analytical methods [10] or numerical ones [11], and their shift-invariance property.

In the regime of computational EMs, scattering by a rough surface always must also be taken into account since it is almost inevitable in practical near-subsurface detection. The Sommerfeld integral method presented in [11] fails to compute Green's functions for a planarly layered medium covered by a rough surface. In addition, the scatterers may be placed across several subsurface planar layers instead of inside a single one and thus the previous work [9] is not consistent with the actual situation. Therefore, in this letter, we focus our work on the EM scattering and inverse scattering from 2-D objects straddling multiple planar layers with a 1-D rough surface. The buried object approach (BOA) proposed in previous works [12], [13] accounting for the EM scattering from the rough surface when 2-D Green's functions are evaluated has been successfully applied to forward scattering [14] and reconstruction [15] of 2-D scatterers buried under a rough surface. Our work further extends these previous works and has the following new contributions.

1) The subsurface structure is allowed to include any number of planar layers while only the half-space model or a limited number of layers beneath the rough surface are considered in the previous works. Our model is closer to the real-world EM scattering scenarios.
2) The 2-D inhomogeneous scatterers can straddle multiple subsurface planar layers in our work. However, they are usually embedded inside one single layer in previous works.
3) The forward scattering computational cost for the scenarios with and without the rough surface is

Qing Wu and Ruidong Huang are with the Institute of Electromagnetics and Acoustics, Key Laboratory of Electromagnetic Wave Science and Detection Technology, Xiamen University, Xiamen 361005, China.

Feng Han is with the School of Computing and Information Technology, Great Bay University, Dongguan, Guangdong 523000, China, and also with the Institute of Electromagnetics and Acoustics, Xiamen University, Xiamen 361005, China (e-mail: feng.han@gbu.edu.cn; feng.han@xmu.edu.cn).

detailedly compared in both theories and numerical results.

4) The permittivity and conductivity parameters of the 2-D scatterers straddling multiple subsurface layers covered by a rough surface are simultaneously reconstructed by the VBIM.

The rest of this letter is organized as follows. In Section II, related theories and methods are briefly introduced. In Section III, the forward scattering computation results are verified by comparing them to the finite element method (FEM) simulations. Meanwhile, we reconstruct the 2-D inhomogeneous profiles straddling several subsurface layers by VBIM and confirm the rough surface effect on the inversion results. Finally, in Section IV, the conclusion is drawn.

II. METHODS

A. One-Dimensional Rough Surface Model

In this work, the 1-D rough surface having the horizontal size L_x is generated from the Gaussian spectrum [16]

$$W(K_x) = \frac{l_x h^2}{2\sqrt{\pi}} \exp\left[-\frac{l_x^2 K_x^2}{4}\right] \tag{1}$$

where $K_x = 2\pi x/L_x$ is the spatial frequency in the $\hat{x}$-direction and l_x is the correlation length in the $\hat{x}$-direction. The parameter h represents the root mean square (rms) height of the rough surface.

B. EM Forward Scattering Model

When multiple planar layers are covered by a 1-D rough surface and the EM wave is in the transverse electric (TE) mode, i.e., the electric field only has the $\hat{y}$ component and is perpendicular to the xz plane, the 2-D state equation still can be formulated by the electric field IE (EFIE)

$$E_y^{\text{inc}}(\boldsymbol{\rho}) = E_y^{\text{tot}}(\boldsymbol{\rho})$$
$$- j\omega\varepsilon_0 \int_D G_{EJ}^{ii}(\boldsymbol{\rho}, \boldsymbol{\rho}')\epsilon_b(\boldsymbol{\rho}')\chi(\boldsymbol{\rho}')E_y^{\text{tot}}(\boldsymbol{\rho}')d\boldsymbol{\rho}' \tag{2}$$

while the data equation is expressed as

$$E_y^{\text{sct}}(\boldsymbol{\rho}) = j\omega\varepsilon_0 \int_D G_{EJ}^{ri}(\boldsymbol{\rho}, \boldsymbol{\rho}')\epsilon_b(\boldsymbol{\rho}')\chi(\boldsymbol{\rho}')E_y^{\text{tot}}(\boldsymbol{\rho}')d\boldsymbol{\rho}'$$
$$\tag{3}$$

where $\boldsymbol{\rho}' = \hat{x}x' + \hat{z}z'$ denotes the source point, $\boldsymbol{\rho} = \hat{x}x + \hat{z}z$ denotes the field point, the background relative complex permittivity ϵ_b is not a constant since the inversion domain D straddles multiple layers, $\chi(\boldsymbol{\rho}) = [\epsilon(\boldsymbol{\rho}) - \epsilon_b(\boldsymbol{\rho})]/\epsilon_b(\boldsymbol{\rho})$ is the contrast of the scatterer, G_{EJ}^{ii} is the Green's function linking $\boldsymbol{\rho}'$ and $\boldsymbol{\rho}$ inside D, and G_{EJ}^{ri} links $\boldsymbol{\rho}'$ inside D and $\boldsymbol{\rho}$ at the receiver array above the rough surface. E_y^{inc}, E_y^{tot}, and E_y^{sct} represent the incident, total, and scattered electric fields, respectively. Before solving for E_y^{tot} from (2) using the BCGS [7], we must compute the incident fields via

$$E_y^{\text{inc}}(\boldsymbol{\rho}) = \int G_{EJ}^{it}(\boldsymbol{\rho}, \boldsymbol{\rho}')J_y(\boldsymbol{\rho}')d\boldsymbol{\rho}' \tag{4}$$

where G_{EJ}^{it} links the $\boldsymbol{\rho}$ inside D and $\boldsymbol{\rho}'$ at the transmitter array which is also located above the rough surface. Once E_y^{tot} is

obtained, we directly substitute it into the data equation (3) and compute the scattered electric fields at the receiver array.

C. Computation of Green's Functions

To account for EM scattering from the 1-D rough surface, we evaluate the three Green's functions G_{EJ}^{it}, G_{EJ}^{ii}, and G_{EJ}^{ri} in (2)–(4) using the BOA which has been adopted in [12], [14], and [15] to deal with the half-space model with a rough surface. The basic idea is to split a Green's function into two parts: the one contributed by the wave reflection and transmission in purely multiple planar layers and the one contributed by the EM scattering from the buried objects of the rough surface embedded in two sides of the first fictitious planar interface. Here, we take G_{EJ}^{ri} as an example and drop the subscript for convenience of formula derivation. It is written as

$$G^{ri}(\boldsymbol{\rho}, \boldsymbol{\rho}') = G_0^{ri}(\boldsymbol{\rho}, \boldsymbol{\rho}') + G_s^{ri}(\boldsymbol{\rho}, \boldsymbol{\rho}') \tag{5}$$

where G_0^{ri} is contributed by the planarly multilayered medium and can be evaluated using the transmission-line analogy method [11]. However, G_s^{ri} corresponds to the EM field scattered from the rough surface and can be obtained by building up another EFIE

$$G_0^{bo,i}(\boldsymbol{\rho}'', \boldsymbol{\rho}') = G_t^{bo}(\boldsymbol{\rho}'')$$
$$- j\omega\varepsilon_0 \int_{RS} G_0^{bo,bo}(\boldsymbol{\rho}'', \boldsymbol{\rho}'')\chi^{bo}(\boldsymbol{\rho}'')G_t^{bo}(\boldsymbol{\rho}'')d\boldsymbol{\rho}''$$
$$\tag{6}$$

where $G_0^{bo,i}$ represents the incident field inside the buried objects when the rough surface is absent while G_t^{bo} represents the total field inside the buried objects when the rough surface is present. And $G_0^{bo,bo}$ is the Green's function in the planarly multilayered medium linking the source point and the field point inside the buried objects. In addition, one should note that, in (6), $\boldsymbol{\rho}'$ is located inside the inversion domain D while $\boldsymbol{\rho}''$ is located inside the buried objects of the rough surface and the subscript RS denotes the rough surface region. χ^{bo} represents the dielectric contrast of the buried objects of the rough surface with respect to the planarly multilayered background medium. We now discretize the buried objects of the rough surface into N_b square pixels and rewrite (6) in a compact matrix form

$$\mathbf{Ax} = \mathbf{b} \tag{7}$$

where

$$\mathbf{A} = \left[\mathbf{I} - j\omega\varepsilon_0\chi^{bo}(\boldsymbol{\rho}_n'')G_0^{bo,bo}(\boldsymbol{\rho}_m'', \boldsymbol{\rho}_n'')\right]\Delta S \in \mathbb{C}^{(N_b, N_b)} \tag{8a}$$
$$\mathbf{x} = \left[G_t^{bo}(\boldsymbol{\rho}_n'')\right] \in \mathbb{C}^{(N_b, 1)} \tag{8b}$$
$$\mathbf{b} = \left[G_0^{bo,i}(\boldsymbol{\rho}_m'', \boldsymbol{\rho}')\right] \in \mathbb{C}^{(N_b, 1)} \tag{8c}$$

in which ΔS is the area of the discretized square pixel and $m, n \in [1, N_b]$ are indexes of the pixels. We then solve for G_t^{bo} from (7) using BCGS and substitute it into the following data equation to compute G_s^{ri} in (5)

$$G_s^{ri}(\boldsymbol{\rho}, \boldsymbol{\rho}') = \sum_{n=1}^{N_b} j\omega\varepsilon_0 G_0^{r,bo}(\boldsymbol{\rho}, \boldsymbol{\rho}_n'')\left[\chi^{bo}(\boldsymbol{\rho}_n'')G_t^{bo}(\boldsymbol{\rho}_n'')\right]\Delta S$$
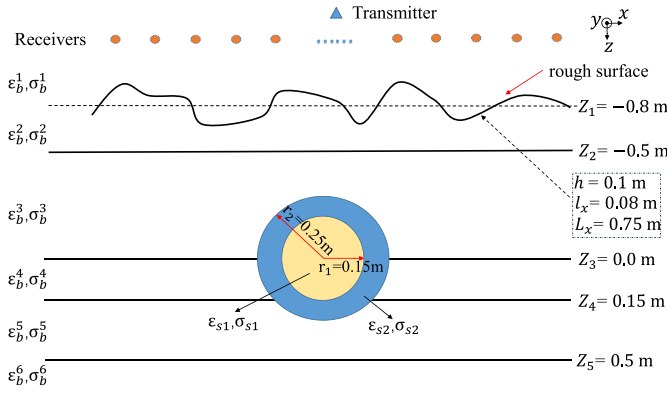$$\tag{9}$$

Fig. 1. Two-layer cylinder with the inner radius $r_1 = 0.1$ m and the outer radius $r_2 = 0.25$ m straddling three planar background layers covered with a locally rough surface. Their geometry parameters are annotated in the figure.
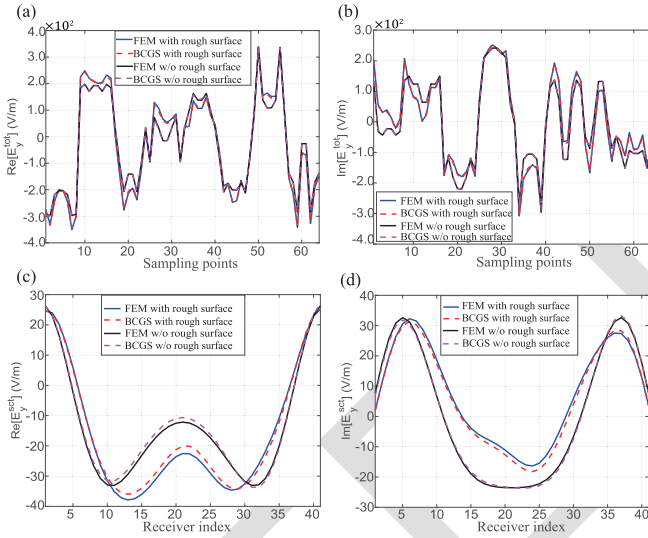

Fig. 2. Comparisons of the solved total electric fields inside the domain enclosing the cylinder and the scattered fields at the receiver array and FEM results when the rough surface is present or absent. (a) Real part of E_y^{tot}. (b) Imaginary part of E_y^{tot}. (c) Real part of E_y^{sct}. (d) Imaginary part of E_y^{sct}.

where $G_0^{r,bo}$ is the planarly multilayered Green's function which links $\boldsymbol{\rho}''$ inside the buried objects of the rough surface and $\boldsymbol{\rho}$ at the receiver array.

D. EM FWI Model

Once the Green's functions are ready, the inversion model almost has no relationship with the rough surface. In this work, we use VBIM with the structural consistency constraint (SCC) to reconstruct 2-D inhomogeneous scatterers straddling multiple planar layers covered by a 1-D rough surface. The detailed implementation of VBIM with SCC for several 3-D cases has been given in [9] and will not be repeated here.

III. NUMERICAL RESULTS

In this section, we verify the correctness of the forward EM scattering solver for 2-D inhomogeneous scatterers placed across multiple subsurface planar layers with a locally rough surface by comparing the BCGS results with the FEM computation via the commercial software COMSOL. Meanwhile, the additional computation cost caused by the rough surface is testified and explained. All the numerical simulations are

TABLE I
MEMORY COST (MB) AND COMPUTATION TIME (S) OF THE FORWARD SOLVER FOR DIFFERENT VARIABLES OR IN DIFFERENT STAGES

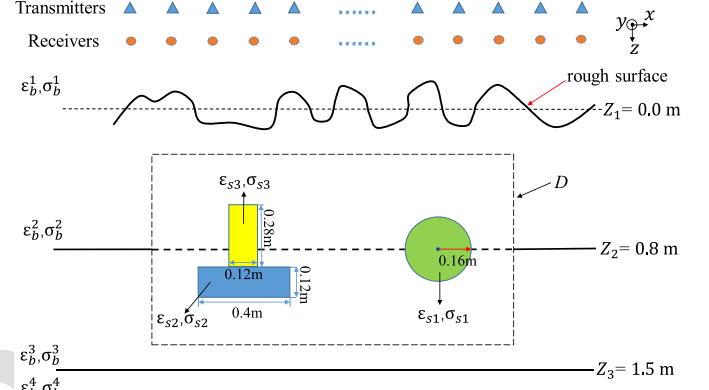|	G_{EJ}^{it} & E_y^{inc}	G_{EJ}^{ii}	BCGS	G_{EJ}^{ri} & E_y^{sct}
Memory w/o rough surface	0.082	6.54	3.49	1.13
Memory with rough surface	5.22	297	99.1	8.35
Time w/o rough surface	2.40	3.51	0.034	5.13
Time with rough surface	17.2	3.67	3.04	4.82

Fig. 3. Configuration of the 2-D inversion model including an inhomogeneous "T" shape scatterer and a homogeneous circular scatterer buried beneath the 1-D rough surface. The scatterers straddle the second and the third layers. Their geometry sizes are annotated in the figure.

performed on a workstation with an 18-core Intel i9-10980XE 3.0 GHz CPU and 256 GB RAM. Finally, we assess the inversion ability of the VBIM solver for multiple 2-D inhomogeneous scatterers straddling multiple planar layers beneath a 1-D rough surface, and also validate the necessity to include the rough surface scattering effect in inversion.

A. Forward Validation

As shown in Fig. 1, the background medium has six layers and the two-layer circular cylinder with its center located at $(0, 0)$ m straddles three layers. The top layer is air and the permeability values of all layers are the same as that of free space μ_0. The relative permittivity values of other layers are $\varepsilon_b^2 = 1.5$, $\varepsilon_b^3 = 2.0$, $\varepsilon_b^4 = 3.0$, $\varepsilon_b^5 = 2.5$, and $\varepsilon_b^6 = 3.0$, respectively. The conductivity values of other layers are $\sigma_b^2 = 1.0$ mS/m, $\sigma_b^3 = 2.0$ mS/m, $\sigma_b^4 = 3.0$ mS/m, $\sigma_b^5 = 2.0$ mS/m, and $\sigma_b^6 = 1.0$ mS/m, respectively. The inner cylinder has the dielectric parameters $\varepsilon_{s1} = 2.5$ and $\sigma_{s1} = 1.0$ mS/m while the outer one has $\varepsilon_{s2} = 4.0$ and $\sigma_{s2} = 3.0$ mS/m. The 2-D line source is located at $(x_s, z_s) = (0, -1.3)$ m. The operation frequency is 1 GHz. Totally, 41 receivers are uniformly located in the horizontal line at $z = -1.1$ m. The coordinate of the 1st receiver is $(-0.6, -1.1)$ m. The distance between two adjacent receivers is 0.03 m. The computational domain enclosing the two-layer cylinder has the dimensions of 0.6×0.6 m. Its center is located at $(0, 0)$ m. The whole region is divided into 60×60 square pixels. Fig. 2 shows the comparisons of total electric fields sampled in 64 uniformly distributed points inside the computational domain and the scattered electric fields at the 41 receivers. We can see that, no matter for EM scattering with or without the rough surface, both the total fields and the scattered fields solved by our BCGS method and FEM match well. The relative errors when the rough surface is present are slightly larger compared with
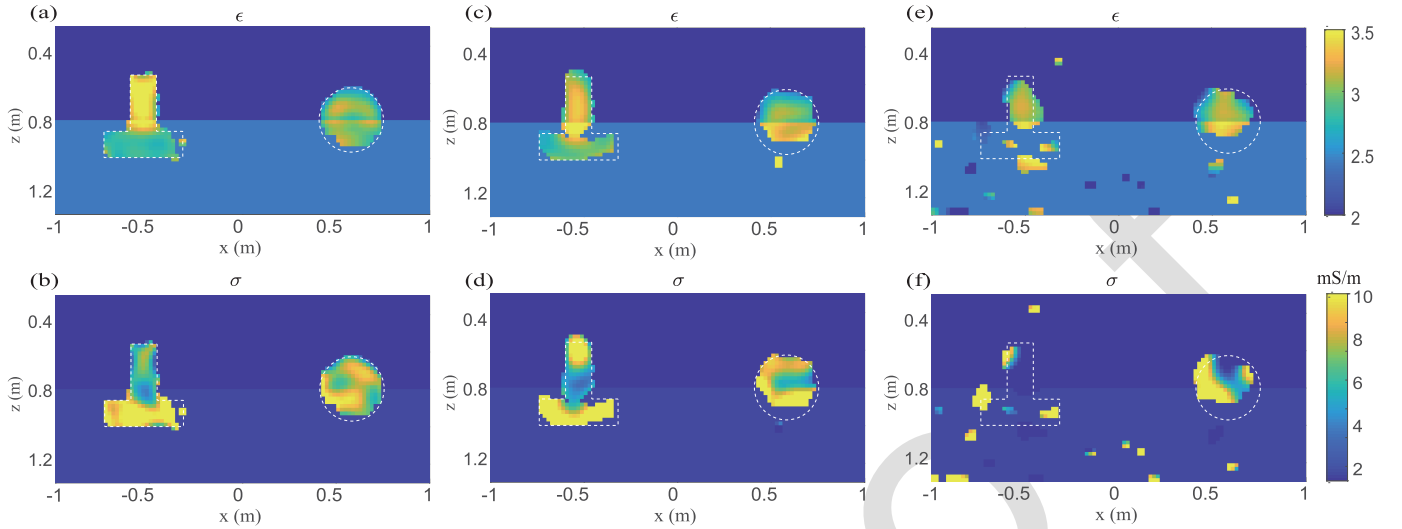
Fig. 4. Reconstructed 2-D profiles of the scatterers which are buried beneath the rough surface and straddle two planar layers. (a) Relative permittivity for $h_{\text{true}} = 0.1$ m and $h_{\text{inv}} = 0.1$ m. (b) Conductivity for $h_{\text{true}} = 0.1$ m and $h_{\text{inv}} = 0.1$ m. (c) Relative permittivity for $h_{\text{true}} = 0.1$ m and $h_{\text{inv}} = 0.1$ m but with 30 dB noise. (d) Conductivity for $h_{\text{true}} = 0.1$ m and $h_{\text{inv}} = 0.1$ m but with 30 dB noise. (e) Relative permittivity for $h_{\text{true}} = 0.1$ m and $h_{\text{inv}} = 0.0$ m. (f) Conductivity for $h_{\text{true}} = 0.1$ m and $h_{\text{inv}} = 0.0$ m. The white dotted boxes denote true shapes.

those when the rough surface is replaced with a flat one. The possible reason is that the additional procedure to solve the IEs to acquire Green's functions for the rough surface scattering leads to additional numerical errors. Table I lists the memory cost and computation time of the forward solver for different variables or in different stages. We can see that the computational resource consumption when the rough surface is present is much higher than that when it is replaced with a flat one. Especially, the BCGS solver taking the rough surface into account spends nearly 90 times time and consumes nearly 30 times memory more than the BCGS-FFT solver for the purely flat surface. The larger memory cost is caused by the additional computation to solve the IE (7) as well as the additional storage to save Green's functions, e.g., G_{EJ}^{ii} since their horizontal shift-invariance is disrupted. This also leads to the failure of FFT acceleration of BCGS and the traditional MoM of course needs more computation time.

B. Inversion Assessment

As shown in Fig. 3, the inversion domain D with the dimensions of 2.0×1.0 m encloses an inhomogeneous "T" shape scatterer and a homogeneous circular disk scatterer. Both scatterers straddle the second and the third layers. Their geometry sizes are annotated in the figure. The dielectric parameters of the disk are $\varepsilon_{s1} = 3.0$, $\sigma_{s1} = 8.0$ mS/m and those of the "T" shape are $\varepsilon_{s2} = 2.8$, $\sigma_{s2} = 10.0$ mS/m and $\varepsilon_{s3} = 3.5$, $\sigma_{s3} = 6.0$ mS/m, respectively. The background medium includes four layers. The first layer is air. The other three subsurface layers have the dielectric parameters $\varepsilon_b^2 = 2.0$, $\sigma_b^2 = 1.0$ mS/m, $\varepsilon_b^3 = 2.4$, $\sigma_b^3 = 1.4$ mS/m, $\varepsilon_b^4 = 3.0$, and $\sigma_b^4 = 2.0$ mS/m, respectively. Totally, 30 transmitters are placed on the $z = -0.4$ m horizontal line. The increment between the two transmitters is 0.4 m. The scattered fields are recorded by 40 receivers which are placed on the $z = -0.3$ m horizontal line. The increment between the two receivers is also 0.4 m. The operation frequency is 300 MHz. The inversion domain D is divided into 100×50 square pixels. In order to filter out the background clutter in the inversion, we adopt

TABLE II
MODEL MISFITS (%) OF THE RECONSTRUCTED 2-D SCATTERERS

Models \ Parameters	ε_r	σ
$h_{true} = 0.1$ m; $h_{inv} = 0.1$ m; noise free	3.08	32.5
$h_{true} = 0.1$ m; $h_{inv} = 0.1$ m; 30 dB noise	5.41	50.2
$h_{true} = 0.1$ m; $h_{inv} = 0.0$ m; noise free	9.44	96.2

VBIM with SCC [9]. Note the efficiency of SCC has been validated in [17] and will not be discussed here. The measured scattered field data recorded at the receiver array are simulated by the BCGS forward solver which has been validated in Section III-A. The model misfit defined in [18, eq. (16)] is used to indicate the inversion performance. In addition, one should note that, although we will use different rms height h values in the following discussion, the same correlation length $l_x = 0.08$ m and horizontal size $L_x = 0.75$ m are set for all cases.

First, let us validate the inversion performance of the VBIM solver for the reconstruction of 2-D inhomogeneous scatterers straddling multiple subsurface planar layers when they are covered by a 1-D locally rough surface. We use h_{true} to denote the true rms height of the rough surface which is adopted by the forward BCGS solver to generate the scattered electric fields. By contrast, we use h_{inv} to denote the rms height used in the inversion model. In this work, it is assumed the rough surface used in the inversion is the same as that of the true model if h_{inv} and h_{true} are the same. Fig. 4(a) and (b), respectively, shows the reconstructed relative permittivity and conductivity profiles for $h_{\text{true}} = h_{\text{inv}} = 0.1$ m. It can be seen that not only the shapes are well reconstructed but also the retrieved dielectric parameters are close to their true values. This is further confirmed by the low model misfit values listed in the second row of Table II. These results indicate that the 2-D VBIM solver is reliable as long as the 1-D rough surface is precisely modeled in the inversion process. The rough surface only influences the computational cost of the forward solver and has little effect on the VBIM solver. In addition, there are

other two interesting observations of the inversion results. One is that the reconstructed conductivity has a worse profile than the permittivity and thus a larger model misfit. The possible reason is the imaginary part of the complex permittivity is much smaller than the real part, thus the scattered field is not sensitive to scatterer conductivity. Another observation is that the layer interface is coupled into the reconstructed profile, which leads to obvious artifacts at the background interface in the inversion. Both the reconstructed "T" shape scatterer and the circular disk show obvious discontinuities near the background interface. This is because the interface also reflects EM waves. As a result, the VBIM solver treats the interface as a scatterer and overlaps it with the true scatterer profile.

Fig. 4(c) and (d) shows the reconstructed relative permittivity and conductivity profiles when 30 dB noise is added for $h_{\text{true}} = h_{\text{inv}} = 0.1$ m. Here, the noise level is defined according to the signal-to-noise ratio (SNR) of power. Compared with the results shown in Fig. 4(a) and (b) for the noise-free case, the obtained shapes of the scatterers show some distortion. This is further confirmed by the larger model misfit values listed in the third row of Table II. Fortunately, the general shapes and positions of the obtained scatterers are reliable. This implies that the VBIM inversion solver for 2-D scatterers straddling multiple subsurface planar layers covered by a rough surface has a certain antinoise ability.

Finally, we try to testify to the necessity to include the accurate rough surface in the inversion. Specifically speaking, we use a purely planar background model, i.e., $h_{\text{inv}} = 0.0$ m in the VBIM inversion process but the true model includes the 1-D rough surface with the rms height $h_{\text{true}} = 0.1$ m. The reconstructed relative permittivity and conductivity profiles in Fig. 4(e) and (f) show large distortions which is also confirmed by the corresponding model misfit values listed in Table II. Especially, the reconstructed conductivity "T" shape almost disappears. Therefore, although treating the real rough surface as a flat one can save implementation time, it may lead to a large distortion of the reconstructed profiles or even a complete failure of inversion.

IV. Conclusion

In this work, for the first time, we solve the 2-D EM forward and inverse scattering problems for inhomogeneous objects straddling multiple subsurface planar layers covered with a 1-D rough surface. The computation accuracy of the forward BCGS solver is validated by comparing its computation results with FEM simulations. Meanwhile, the influence of the rough surface on the forward and inverse solvers is also investigated. The rough surface significantly increases both the memory cost and computation time in the forward scattering due to the additional IE used for solving Green's functions and the disruption of their horizontal shift-invariance. Unfortunately, neglecting the rough surface in the inversion will lead to obvious reconstructed profile distortion or even implementation failure. The future work will be focused on the improvement of the computation efficiency. One possible solution is using the surface IE instead of the volume IE to formulate the

state equation like (6) to account for rough surface scattering since the fictitious objects of the rough surface are usually homogeneous.

References

[1] G. Mie, "Contributions to the optics of turbid media, particularly of colloidal metal solutions," *Ann. Phys.*, vol. 25, no. 3, pp. 377–445, Feb. 1976.

[2] K. Agarwal, L. Pan, and X. Chen, "Subspace-based optimization method for reconstruction of 2-D complex anisotropic dielectric objects," *IEEE Trans. Microwave Theory Techn.*, vol. 58, no. 4, pp. 1065–1074, Apr. 2010.

[3] Q. Huo Liu et al., "Active microwave imaging. I. 2-D forward and inverse scattering methods," *IEEE Trans. Microwave Theory Techn.*, vol. 50, no. 1, pp. 123–133, Jan. 2002.

[4] K. Yang, C. Torres-Verdín, and A. E. Yilmaz, "Detection and quantification of three-dimensional hydraulic fractures with horizontal borehole resistivity measurements," *IEEE Trans. Geosci. Remote Sens.*, vol. 53, no. 8, pp. 4605–4615, Aug. 2015.

[5] G. K. Avdikos and H. T. Anastassiu, "Computational cost estimations and comparisons for three methods of applied electromagnetics (MoM, MAS, MMAS)," *IEEE Antennas Propag. Mag.*, vol. 47, no. 1, pp. 121–129, Feb. 2005.

[6] Z. Q. Zhang and Q. H. Liu, "Three-dimensional weak-form conjugate- and biconjugate-gradient FFT methods for volume integral equations," *Microwave Opt. Technol. Lett.*, vol. 29, no. 5, pp. 350–356, Jun. 2001.

[7] F. Han, J. Zhuo, N. Liu, Y. Liu, H. Liu, and Q. H. Liu, "Fast solution of electromagnetic scattering for 3-D inhomogeneous anisotropic objects embedded in layered uniaxial media by the BCGS-FFT method," *IEEE Trans. Antennas Propag.*, vol. 67, no. 6, pp. 1748–1759, Mar. 2019.

[8] W. Zhang and Q. H. Liu, "Three-dimensional scattering and inverse scattering from objects with simultaneous permittivity and permeability contrasts," *IEEE Trans. Geosci. Remote Sens.*, vol. 53, no. 1, pp. 429–439, Jan. 2015.

[9] J. Zhuo, L. Ye, F. Han, L. Xiong, and Q. H. Liu, "Multiparametric electromagnetic inversion of 3-D biaxial anisotropic objects embedded in layered uniaxial media using VBIM enhanced by structural consistency constraint," *IEEE Trans. Antennas Propag.*, vol. 68, no. 6, pp. 4774–4785, Jun. 2020.

[10] A. Abubakar and T. M. Habashy, "A closed-form expression of the electromagnetic tensor Green's functions for a homogeneous TI-anisotropic medium," *IEEE Geosci. Remote Sens. Lett.*, vol. 3, no. 4, pp. 447–451, Oct. 2006.

[11] K. A. Michalski and J. R. Mosig, "Multilayered media green's functions in integral equation formulations," *IEEE Trans. Antennas Propag.*, vol. 45, no. 3, pp. 508–519, Mar. 1997.

[12] Y. Altuncu, A. Yapar, and I. Akduman, "Buried object approach for solving scattering problems related to rough surfaces," *Can. J. Phys.*, vol. 85, no. 1, pp. 39–55, Jan. 2007.

[13] Y. Altuncu, A. Yapar, and I. Akduman, "Numerical computation of the green's function of a layered media with rough interfaces," *Microwave Opt. Technol. Lett.*, vol. 49, no. 5, pp. 1204–1209, 2007.

[14] Y. Altuncu, A. Yapar, and I. Akduman, "On the scattering of electromagnetic waves by bodies buried in a half-space with locally rough interface," *IEEE Trans. Geosci. Remote Sens.*, vol. 44, no. 6, pp. 1435–1443, Jun. 2006.

[15] T. U. Gurbuz, B. Aslanyurek, E. P. Karabulut, and I. Akduman, "An efficient nonlinear imaging approach for dielectric objects buried under a rough surface," *IEEE Trans. Geosci. Remote Sens.*, vol. 52, no. 5, pp. 3013–3022, May 2014.

[16] L. Tsang, J. A. Kong, and K.-H. Ding, *Scattering of Electromagnetic Waves: Theories and Applications*. Hoboken, NJ, USA: Wiley, 2000, ch. 9.

[17] J. Li, J. Zhuo, Z. Guan, F. Han, and Q. H. Liu, "3-D electromagnetic scattering and inverse scattering by magnetodielectric objects with arbitrary anisotropy in layered uniaxial media," *IEEE Trans. Antennas Propag.*, vol. 68, no. 2, pp. 1009–1022, Feb. 2020.

[18] T. Lan, N. Liu, F. Han, and Q. H. Liu, "Joint petrophysical and structural inversion of electromagnetic and seismic data based on volume integral equation method," *IEEE Trans. Geosci. Remote Sens.*, vol. 57, no. 4, pp. 2075–2086, Apr. 2019.